Pergamon

Int. J. Heat Mass Transfer. Vol. 38, No. 11, pp. 1933–1944, 1995

0017-9310/95 $9.50+0.00

0017-9310(94)00334-3

Cooling of optical fiber in aiding and opposing forced gas flow

THEODOROS VASKOPULOS, CONSTANTINE POLYMEROPOULOS† and ABDELFATTAH ZEBIB

Department of Mechanical and Aerospace Engineering, Rutgers, The State University of New Jersey, P.O. Box 909, Piscataway, NJ 08855, U.S.A.

(*Received* 9 *March* 1994 *and in final form* 19 *October* 1994)

Abstract—Convective flows in annular passages with the inner core moving at constant speed were investigated for conditions applied to the cooling of optical fiber during the draw process. Temperature dependent gas properties were fully accounted for in the complete set of conservation equations. The geometrical configuration of the model was formulated to reflect experimental conditions previously used for cooling of the fiber in forced flow. The numerical solution of the conservation equations was validated using experimental measurements. The numerical results were used to predict the variation of fiber temperature at the cooling section exit with respect to relevant draw parameters for aiding and opposing flows. A mean temperature for the gas properties was found, that can be used to predict within 10% the exit fiber temperature using constant property modeling. The results presented allow estimation of the fiber temperature for a wide range of operating conditions and cooling section geometries.

1. INTRODUCTION

During the process of drawing optical fiber from a glass rod the fiber must cool to a temperature low enough to be compatible with the properties of the coating material. Considering as the initial temperature of the fiber that at the end of neckdown, where it reaches its final diameter (commonly taken to be the glass softening point around 1600°C), cooling of the fiber to the required final temperature of around 100°C may not be possible by means of only the convective field around the hot moving surface. This cooling mode, which may be called natural cooling, is not adequate for high fiber draw speeds unless a tall draw tower is used. However, tall towers are expensive to build and operate. On the other hand, high production rate requires high draw speeds, and as a consequence accelerated fiber cooling becomes a necessary consideration for the drawing process. This can be achieved by means of forced convection using an external gas flow with respect to the fiber surface. This cooling mode may be called forced fiber cooling.

The prediction of natural cooling of optical fiber has been considered by Glicksman [1] using the Reynolds analogy, and by Bourne and Elliston [2], Bourne and Dixon [3], and by Karniš and Pechoč [4], using integral methods. Comparison of the Bourne and Elliston [2] predictions with the experimental data of Arridge and Prior [5] showed good agreement subject to the choice of a suitable temperature for the computation of physical properties. Using the experimental data of Arridge and Prior [5] and Maddison and McMillan [6], Paek and Schroeder [7] estimated mean heat transfer coefficients for fiber natural cooling in air from the neckdown to the ambient temperature. Experimental data by Kyriacou *et al.* [8] confirmed the empirical heat transfer coefficients of Paek and Schroeder [7]. The experiments of Jochem and Van der Ligt [9] showed that changing the ambient air environment to helium or hydrogen can substantially increase the fiber cooling rate. Similar experimental results were also reported by Vasiliev *et al.* [10].

Forced cooling of the fiber was reported by Paek and Schroeder [7], who directed a gas stream transverse to the moving fiber. This cooling technique, however, is limited by the accompanying oscillations of the fiber. To avoid this problem Kyriacou *et al.* [8] used helium flow in a tube in a direction opposing the fiber motion and showed considerable cooling improvement compared to that with transverse gas flow. Vaskopulos *et al.* [11] and Vaskopulos [12] used a similar opposing flow cooling section to experimentally assess the influence of cooling gas flow rate, cooling section diameter, wall temperature, and cooling gas composition on fiber temperature. Vaskopulos *et al.* [11] showed that numerical integration of the full constant property conservation equations using an algorithm based on the SIMPLER method could be used to predict the fiber temperature at the cooling section exit. This was subject to using an appropriate mean temperature for the gas property estimation. However, because of the large gas temperature variation within the cooling section, *a priori* estimation of such a mean gas temperature was not feasible and the constant gas temperature results were considered of qualitative significance. Results from numerical inte-

† Author to whom correspondence should be addressed.

NOMENCLATURE

c_p	specific heat
D	diameter
g	gravity constant
Gr	Grashof number, $g\lvert\rho_{fin}-\rho_w\rvert(D_w-D_f)^3/\rho_{fin}v_w^2$
h	heat transfer coefficient
k	thermal conductivity
L	cooling section length
Nu	local Nusselt number, $h(D_w-D_f)/k_w$
p	pressure
p_0	ambient pressure
Pe	fiber Peclet number, $\rho_f c_{pf} D_f V_f/k_f$
Pr	Prandtl number, $\mu_w c_{pw}/k_w$
r	radial coordinate
R	gas constant
Re	Reynolds number, $\rho_w V_m(D_w-D_f)/\mu_w$
T	temperature
u	velocity in the radial direction
u_{in}	cooling gas inlet speed
v	velocity in the axial direction
V	velocity
X	distance from glass softening point location
z	axial coordinate.

Greek symbols

θ	dimensionless temperature, $T-T_w/T_{fin}-T_w$
μ	dynamic viscosity
v	kinematic viscosity
ρ	density.

Superscript

$'$	dimensionless variables (except θ).

Subscripts

fin	fiber entrance
f	fiber
m	mean
out	outlet of cooling section
w	cooling section wall.

gration of the conservation equations for aiding and opposing gas flows with constant gas properties were also presented by Choudhury and Jaluria [14]. They showed the effect of a range of flow and geometric parameters on the fiber cooling process, but for cooling section length to diameter, and cooling section diameter to fiber diameter ratios that were too small to apply to the processes related to the experiments with forced fiber cooling.

There is a large body of reported work on cooling of moving plates or cylinders which is related, but not entirely appropriate to fiber cooling, because of the geometries considered, the approximations involved in the model equations, and the flow conditions used [15–24]. Annular aiding flows using the full governing equations for the conjugate flow with a moving flat inner surface were considered by Kang *et al.* [25], and Choudhury and Jaluria [26].

The present work presents results from an investigation appropriate to the cooling of optical fibers with mixed convection in an annular geometry. A comprehensive model using the full governing conservation equations, including variable gas properties, is considered. The model geometry was motivated by the fiber cooling section designed for the experimental portion of the work with fiber cooling in an actual draw tower. The conservation equations were integrated using an efficient computer code, and experimental results were used to validate the numerical predictions. Extension of the computed results to a wide range of relevant input parameters led to an understanding of the cooling process and enable the design of a fiber cooling section satisfying specific needs. The present paper is based on the results of Vaskopulos [12]. It extends previous work [13], including additional experimental data, discussion of aiding and opposing flows, as well as computed results that can be used for estimation of cooling section performance. Comparison of the results using variable and constant cooling gas properties also enables the definition of a mean temperature for gas property estimation which can yield reasonable prediction of the fiber temperature at the exit of the cooling section using constant property analysis.

2. EXPERIMENTAL APPARATUS

Details of the experimental apparatus can be found elsewhere [11, 12]. Only a brief description will be given here to enable an easier understanding of the chosen geometry and of the discussion of the computational work. Figure 1 is a schematic diagram showing the main components of the apparatus. The cooling section was an aluminum water-cooled 0.5 m long tube, equipped with interchangeable inserts for varying the fiber passage diameter from 4 to 8 mm. The cooling section was connected to two 5 cm long cylindrical plenum chambers attached on either side of the tube. The cooling gas was introduced into the gas inlet chamber, which was kept at atmospheric pressure, monitored by a pressure sensor, to minimize gas losses through the opening at the fiber exit. Thus the only gas loss was due to the Couette type flow caused by the fiber motion in the 4 mm diameter lower fiber exit passage. The vacuum plenum chamber was maintained at pressure below atmospheric using a vacuum pump, thus creating the necessary pressure difference through the fiber passage for the desired

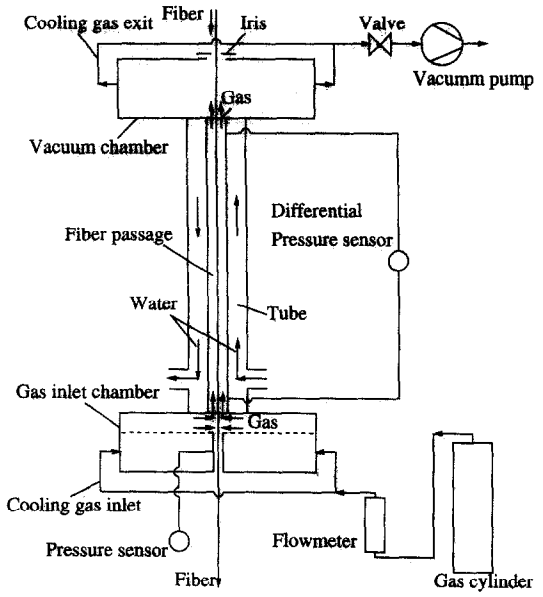

Fig. 1. Schematic diagram of the cooling apparatus for opposing flow.

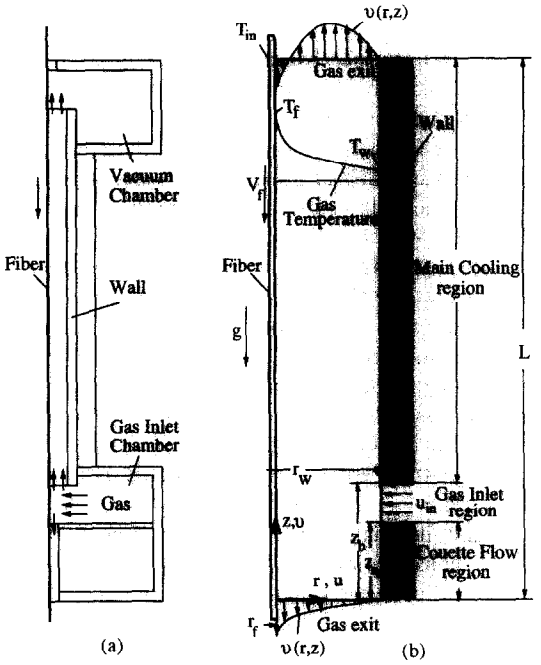

Fig. 2. Opposing flow. Schematic diagram of the experimental apparatus and the corresponding numerical model.

gas flow. The gas flow rate was controlled by monitoring the pressure difference across the cooling section using a differential pressure sensor and a calibration curve between the pressure difference and the gas flow rate. The calibration curve was obtained experimentally with stationary fiber through the cooling section. The accuracy of the flow rate, including the error associated with the fiber motion during the fiber drawing, was estimated to be ± 0.3 l min^{-1}. As it will be shown later, however, the fiber temperature did not vary significantly with gas flow rate. Cooling gases were pure helium, as well as helium–nitrogen mixtures. The fiber temperature was measured at a fixed point 15 cm downstream from the apparatus using a commercial non-contact fiber temperature sensor. Figure 1 shows the fiber moving in a direction opposing the gas flow. Cooling with aiding flow could also be tested by mounting the apparatus in an inverted position. For all tests the cooling section was placed 54 cm downstream from the draw tower heater. The fiber was drawn from a preform using a commercial 6.9 m draw tower with graphite heating elements and equipped with the necessary controls for the fiber diameter and the draw rate. The fiber diameter was 150 μm and the draw speed ranged from 1 to 3 m s^{-1}.

3. MODEL, GOVERNING EQUATIONS AND NUMERICAL SOLUTION

The fiber cooling process was modeled to reflect the geometry used in the experimentation, and Fig. 2 is a diagram of the model shown side by side with the cooling section. The model consisted of an annular passage of circular cross section with an outer surface at constant temperature, representing the cooling section wall. The inner surface, representing the fiber, was moving axially at a constant speed. Figure 2 shows the inner surface motion opposing the gas flow, but aiding flows were also allowed. The inner surface temperature varied axially, depending on the rate of heat transfer to the cooling gas. The cooling gas entered sideways at the gas inlet region, and flowed towards the main cooling region under the influence of a pressure difference. In the Couette flow region the gas flow was controlled by the fiber motion only, since, as in the experimental apparatus, the pressure drop was negligible. The side entrance simulated the entrance of the cooling gas in the gas inlet chamber of the test section. In addition, it avoided the difficulty encountered with an axial cooling gas entrance in the formulation of the correct inflow boundary conditions for opposing flow operation.

Principal model assumptions were (a) steady, axisymmetric laminar flow, (b) radially lumped fiber temperature [the fiber Biot number was $O(10^{-2})$], (c) negligible axial conduction in the fiber [the fiber Peclet number was $O(10^2)$], (d) no viscous dissipation or pressure work, and (e) no heat transfer by thermal radiation.

Regarding assumption (a) for the axisymmetric annular flows considered, where the inner surface may aid or oppose the gas flow, the limits for laminar flow are not known. It should be expected, however, that as the gas flow rate or the fiber speed increase, laminar flow model predictions should show departure from the measured results. Assumptions (b) and (c) can safely be employed for modeling the cooling of optical fiber, which is usually 100–150 μm in diameter, with draw speeds over 0.5 m s^{-1}. Assumption (d) is appro-

priate to the low cooling gas speeds employed. Neglecting heat transfer by radiation [assumption (e)], even at the high fiber temperatures right after the neckdown region, can be justified on the basis of the very low spectral emittance of fused silica in the wavelength range below approximately 3 μm, where the glass is practically transparent to thermal radiation [27]. For lower temperatures the emitted radiation is shifted to longer wavelengths where the spectral emittance of the fiber is expected to be considerably less than unity [27]. However, there is currently insufficient information to estimate the actual spectral dependence in the fiber diameter range of interest. Nevertheless, it is possible to show from the results of the present calculations that, for fiber temperatures relevant to the present work, the expected radiant flux from a fiber with unit emittance is more than an order of magnitude smaller than the convected heat flux.

The conservation equations with temperature dependent properties were written in conservative dimensionless form as follows:

continuity equation

$$\frac{1}{r'}\frac{\partial}{\partial r'}(r'\rho'u')+\frac{\partial}{\partial z'}(\rho'v')=0 \tag{1}$$

radial momentum equation

$$\frac{1}{r'}\frac{\partial(r'\rho'u'u')}{\partial r'}+\frac{\partial(\rho'v'u')}{\partial z'}=-\frac{\partial p'}{\partial r'}+\frac{1}{Re}\left[\frac{1}{r'}\frac{\partial}{\partial r'}\left[2r'\mu'\frac{\partial u'}{\partial r'}-\tfrac{2}{3}r'\mu'\left(\frac{\partial u'}{\partial r'}+\frac{u'}{r'}+\frac{\partial v'}{\partial z'}\right)\right]+\frac{\partial}{\partial z'}\left[\mu'\left(\frac{\partial u'}{\partial z'}+\frac{\partial v'}{\partial r'}\right)\right]+\frac{2\mu'}{r'}\left(\frac{\partial u'}{\partial r'}-\frac{u'}{r'}\right)-\frac{2\mu'}{r'}\left[\frac{\partial u'}{\partial r'}-\frac{1}{3}\left(\frac{\partial u'}{\partial r'}+\frac{u'}{r'}+\frac{\partial v'}{\partial z'}\right)\right]\right] \tag{2}$$

axial momentum equation

$$\frac{1}{r'}\frac{\partial(r'\rho'u'v')}{\partial r'}+\frac{\partial(\rho'v'v')}{\partial z'}=-\frac{\partial p'}{\partial z'}+\frac{1}{Re}\left[\frac{1}{r'}\frac{\partial}{\partial r'}\left[\mu'r'\left(\frac{\partial u'}{\partial z'}+\frac{\partial v'}{\partial r'}\right)\right]+\frac{\partial}{\partial z'}\left[2\mu'\frac{\partial v'}{\partial z'}-\tfrac{2}{3}\mu'\left(\frac{\partial u'}{\partial r'}+\frac{u'}{r'}+\frac{\partial v'}{\partial z'}\right)\right]\right]\pm\frac{Gr}{Re^2}\theta\rho' \tag{3}$$

energy equation

$$c_p'\left(\frac{\partial(r'\rho'u'\theta')}{\partial r'}+\frac{\partial(\rho'v'\theta)}{\partial z'}\right)=\frac{1}{RePr}\times\left[\frac{1}{r'}\frac{\partial}{\partial r'}\left(r'k'\frac{\partial\theta}{\partial r'}\right)+\frac{\partial}{\partial z'}\left(k'\frac{\partial\theta}{\partial z'}\right)\right]. \tag{4}$$

The sign of the last term of the axial momentum equation was (+) for aiding flow and (−) for opposing flow. The ideal gas equation ($p=\rho RT$) was used for the computation of the gas density. The variation of the gas properties with temperature was evaluated using the data in ref. [28]. The glass properties used in all calculations were $\rho_f = 2200$ kg m^{-3}, $k_f = 1.984$ W m^{-1} K^{-1} and $c_{pf} = 1045$ J kg^{-1} K^{-1} and were assumed constant. The boundary conditions for opposing flow are given below:

$$\text{at } z'=0 \quad \frac{\partial u'}{\partial z'}=0 \quad v'=-V_f'\frac{\log r'}{\log r_f'} \quad \frac{\partial^2\theta}{\partial z'^2}=0$$

$$\text{at } z'=L' \quad \frac{\partial u'}{\partial z'}=0 \quad \frac{\partial v'}{\partial z'}=0 \quad \frac{\partial^2\theta}{\partial z'^2}=0$$

$$\text{at } r'=r_f' \quad u'=0 \quad v'=-\frac{V_f}{V_m}$$

$$\frac{\partial\theta}{\partial z'}=-\frac{k'(\theta)}{Pe}\frac{\partial\theta}{\partial r'} \quad \text{at} \quad z=L' \quad \theta=1$$

$$\text{at } r'=r_w' \quad \text{for } 0<z'<L' \quad \theta=0 \quad \text{and} \quad v'=0$$

$$\text{for } 0<z'<z_a' \quad \text{and } z_b'<z'<L', u'=0$$

$$\text{for } z_a'<z'<z_b', u'=\frac{-u_{in}}{V_m}.$$

The same boundary conditions were used for aiding flow with exception that $\theta = 1$ at $z = 0$. The inlet fiber temperature, T_{fin}, depended on the natural cooling of the fiber from the draw tower heater to the cooling section entrance. Natural fiber cooling was accounted for using empirically derived heat transfer coefficients [7] and the following relationship:

$$\frac{T_{fin}-T_\infty}{T_g-T_\infty}=\exp\left(-\frac{4hX}{Pe\,k_f}\right) \tag{5}$$

where T_g was set equal to 1600°C at the end of the neckdown region. X was the distance between the end of neckdown and the entrance to the cooling section.

The dimensionless parameters in the equations were defined as follows:

$$p'=\frac{p-p_o}{\rho_w V_m^2} \quad r'=\frac{r}{D_w-D_f} \quad z'=\frac{z}{D_w-D_f} \quad u'=\frac{u}{V_m} \quad v'=\frac{v}{V_m}$$

$$L'=\frac{L}{D_w-D_f} \quad r_f'=\frac{\frac{D_f}{2}}{D_w-D_f} \quad r_w'=\frac{\frac{D_w}{2}}{D_w-D_f} \quad \theta=\frac{T-T_w}{T_{fin}-T_w}$$

$$\rho'=\frac{\rho}{\rho_w} \quad \mu'=\frac{\mu}{\mu_w} \quad k'=\frac{k}{k_w} \quad c_p'=\frac{c_p}{c_{pw}}.$$

The system of equations and the boundary conditions were numerically integrated using a finite volume algorithm based on the SIMPLER algorithm described by Patankar [29]. The boundary conditions at $z' = 0$ and $z' = L'$ were applied at artificial extensions of the numerical domain. The length of the extensions was sufficient so not to affect the outcome of the numerical results. The code subroutines were fully vectorizable using the zebra ordering technique. The convergence criterion was based on the normalized residuals of the discretized equations so that the larger of the residuals was less than 10^{-9}. The

error in the global mass and energy balances must also have been less than 0.1%. Each iteration took 1.7 s in a CONVEX C1 computer and an average of 400 iterations were required for convergence.

4. RESULTS AND DISCUSSION

4.1. *Model validation*

Validation of the model results was carried out by comparison with experimental data obtained using the fiber cooling apparatus. Figure 3 shows examples of computed and measured fiber exit temperatures, T_{out}, at a position 15 cm below the cooling apparatus exit, corresponding to the location of the fiber temperature sensor. Given the large fiber temperature variation over which the computations were carried out, the agreement between measured and the computed results was very good.

Similar very good agreement between computed and experimental results for both opposing and aiding flows was found using additional experimental data [12], including different cooling section diameters (4 and 8 mm), different cooling gases (pure helium, pure nitrogen and 50% by mass helium–nitrogen mixtures), different cooling wall temperatures (4 and 25°C), different fiber speeds (1.67–3 m s^{-1}) and cooling gas flow rates. The good agreement enables extending model predictions to conditions different than those tested.

In all subsequent figures, unless otherwise noted, the cooling gas was helium, the fiber radius, r_f, was 150 μm, the wall temperature, T_w, was 25°C, the cooling section length, L, and diameter, D_w, were 0.604 m and 8 mm, respectively, and the distance of the cooling section from the furnace was 0.54 m. The fiber temperature was computed at a distance of 1.29 m from the position where the fiber is at the glass softening point (1600°C).

4.2. *Influence of the Reynolds number and the flow direction*

Figure 3(a) and (b), which was used to discuss validation of the model, also shows the variation of the fiber exit temperature, T_{out}, with Reynolds number, Re. As defined in the present work Re is proportional to the flow rate of gas through the main cooling region. For opposing flow the total flow introduced at the side entrance was not equal to the flow through the main cooling region, since a portion was carried out by the fiber as it exited the apparatus. The fraction of the inlet flow through the main cooling region depended on the fiber speed and varied between 82 and 46% for fiber speeds between 2 and 12 m s^{-1}.

Figure 3(a) shows that the effect of Re on T_{out} was relatively small, with the fiber temperature at the cooling section exit decreasing with increasing flow rate for opposing flows. Similar results regarding the small influence of Re on the magnitude of the fiber exit temperature were also found for aiding flows. However, Fig. 3(b) shows that for aiding flows T_{out} increased slightly with Re. This was a consequence of the fact that the cooling section was of sufficient length so that, for the conditions tested, the mean cooling gas temperature at the exit eventually increased with gas flow rate. This is because, after initially being heated up by the hot fiber, the gas must eventually approach the cooling section wall temperature, and the time for cooling is reduced with increasing flow rate. The increase in mean cooling gas temperature as the flow rate increased in turn reduced the heat transfer rate from the fiber, resulting in higher fiber temperatures. It should be noted that this result depends on the length of the cooling section, and that for shorter cooling sections with aiding flow the fiber temperature can be shown to decrease with increasing gas flow rate [12]. For conditions typical of those considered in this paper, Fig. 3(c) is a comparison of the computed fiber temperature, T_{out}, for aiding and opposing flows, and shows that opposing flows resulted in fiber exit temperatures which were lower than those obtained with aiding flow. For this reason the subsequent discussion will concentrate mostly on opposing flow results, but substantial differences with aiding flows will also be pointed out. More detailed results can be found in ref. [12].

A local Nusselt number, Nu, that includes the temperature dependent gas conductivity can be defined as follows:

$$Nu = \left(\frac{1}{T - T_w} \frac{\partial T}{\partial r} \frac{k(T)}{k_w} \right)_{r=r_f} = \frac{h(D_w - D_f)}{k_w}. \quad (6)$$

Figure 4a shows the computed variation of Nu along the cooling section for three different values of Re and for opposing flow. The cooling gas entrance was at $5 < z' < 6$ and the fiber entrance at $z' = 76$. The spikes shown in Fig. 4(a) are at the position of the cooling gas entrance and they are a consequence of increased heat transfer as the cooling gas entering from the side was forced near the fiber. Beyond the gas entrance, Nu initially decreased as the flow developed, and then it increased toward the fiber entrance. The increase of Nu as the fiber entrance was approached was a result of the increase of the gas thermal conductivity as the temperature increased towards the fiber entrance. Previous constant gas property calculations yielded a constant fully developed flow Nu, whose magnitude depended on the assumed property temperature downstream from the cooling gas entrance. The effect of increasing Re in Fig. 4(a) was to increase the local Nu by a relatively small amount, which is consistent with the previously noted small decrease in fiber exit temperature with increase in flow rate in opposing flows.

Figure 4(b) shows the variation of Nu for aiding flow. In this case Nu decreased away from the gas entrance because of the decrease of the gas thermal conductivity as the fiber was cooled, while moving in the gas flow direction. The curves for different Re in Fig. 4a cross inside the main cooling region, resulting

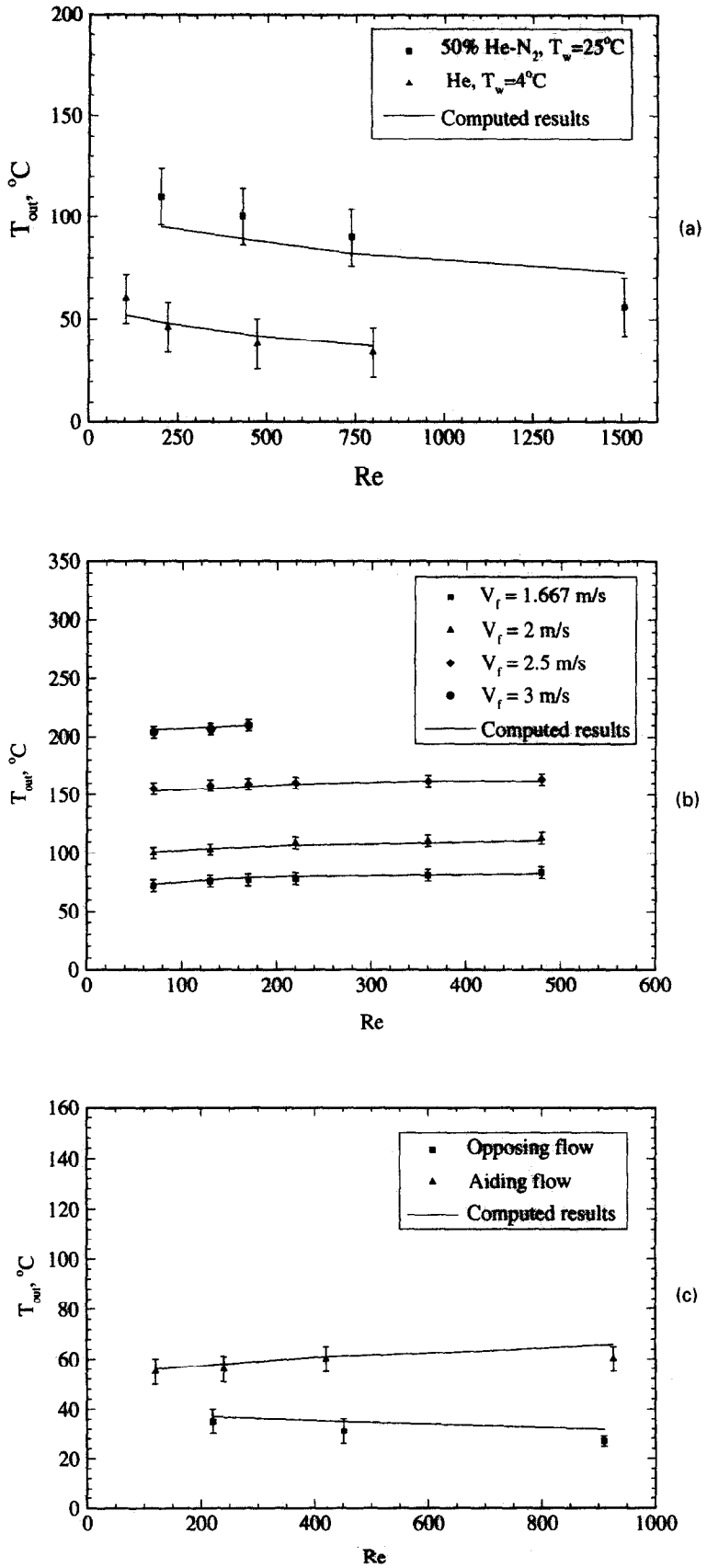

Fig. 3. Comparison between experimental and computed results. (a) Opposing flow ($D_w = 8$ mm, $V_f = 2$ m s^{-1}); (b) aiding flow ($D_w = 8$ mm, $T_w = 25$°C, helium); (c) aiding and opposing flow ($D_w = 4$ mm, $V_f = 1.67$ m s^{-1}, $T_w = 25$°C, helium).

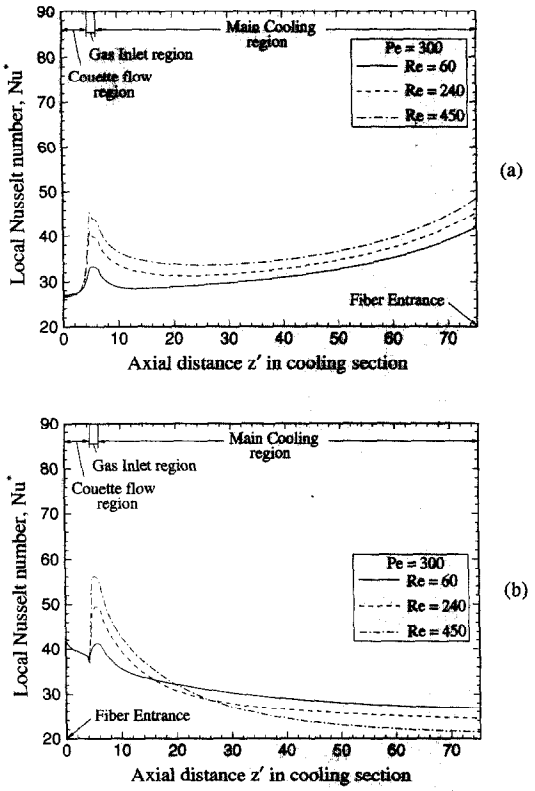

Fig. 4. Variation of local Nu inside the cooling section for different Re. (a) Opposing flow, (b) aiding flow.

in decrease of Nu with increasing Re for most part of the main cooling region, which is in agreement with the results of Fig. 3b regarding the increase of fiber exit temperature with increasing Re for aiding flows.

Figure 5 shows flow streamlines and iso-temperature areas within the cooling section for $Re = 40$ and 210, respectively. Introducing the cooling gas in a direction opposing the fiber motion resulted in a region with flow reversal whose position and size depended on the flow rate. Increasing Re was equivalent to increasing the side entrance flow rate as well as the flow rate into the main cooling region. As shown in Fig. 5, this resulted in decreasing the overall size of the flow reversal region as well as moving it closer to the fiber surface. The net effect was the increase in the heat transfer rate from the fiber with increasing Re, as noted by the results in Fig. 6. For aiding flow there was no flow reversal [12]. Similar behavior was noted by Choudhury and Jaluria [14].

Although the buoyancy term was included in the numerical computation, the influence of free convection was negligible for the range of conditions considered. The ratio Gr/Re^2, which can be used to denote the influence of free convection, was of the order of 10^{-2}.

4.3. *Effect of fiber speed*

Figure 6 shows the dimensionless fiber exit temperature, θ_{out}, plotted as a function of Pe for aiding and opposing flows. The variation of fiber speed is expressed in terms of the fiber Peclet number, Pe, which is proportional to the fiber speed, V_f and fiber diameter, D_f. The fiber speed affects the fiber temperature because of its impact on the fiber cooling time. It also influences the fiber temperature, T_{fin}, at the inlet of the cooling apparatus which in turn impacts on the temperature dependent properties of the gas. In addition, viscous drag around the moving fiber affects significantly the cooling section gas flow field. The Peclet number variation shown corresponds to fiber speeds from approximately 1.7 to 12 m s^{-1} for the present cooling apparatus. The results in Fig. 6 show a significant increase in fiber temperature with increasing fiber speed and the advantage of using opposing flow. Figure 6 also shows fiber temperatures, θ_{out}, computed considering natural cooling only, and points to the significant benefits expected using the present forced cooling method.

4.4. *Effect of cooling section wall diameter*

The effect of changing the cooling section wall diameter D_w is shown in Fig. 7, where the fiber exit temperature θ_{out} is plotted against D_w for four different values of Pe. Increasing the wall diameter, all other conditions remaining the same, effectively reduces the temperature gradients near the fiber, resulting in lower heat transfer from the fiber and higher fiber temperature. According to Fig. 7, the fiber exit temperature can be reduced to a low level using a cooling section with small fiber passage. However, the optimum wall diameter D_w will also depend on the minimum acceptable clearance to avoid physical contact between the fiber and the wall due to small but unavoidable fiber vibrations and to misalignment of the fiber in the narrow cooling section passage. Figure 7 also shows that, for high enough values of D_w, the rate of increase of θ_{out} with D_w decreases. This is expected because for sufficiently large values of D_w, θ_{out} will asymptotically reach a value resulting when only natural cooling is considered.

4.5. *Effect of cooling section wall temperature*

Previous experimental work [11, 12] showed that changing the cooling wall temperature, T_w, from 4 to 25°C resulted in an almost equivalent change in fiber temperature at the cooling section exit. The effect of changing wall temperature on the computed temperature, θ_{out}, is through the temperature dependent gas properties. Figure 8 shows the influence of T_w on θ_{out} for three cooling wall diameters and for two Peclet numbers. For the relatively small range of T_w values around the ambient temperature that are practically attainable, Fig. 8 shows that the computed values of θ_{out} were weakly dependent on T_w according to the relationship:

$$\theta_{out} = 0.0002 \times (T_w - 25) + \theta_{out}|_{\text{at } T_w = 25\,^\circ\text{C}}. \quad (7)$$

Equation (7) was derived for $300 < Pe < 2100$,

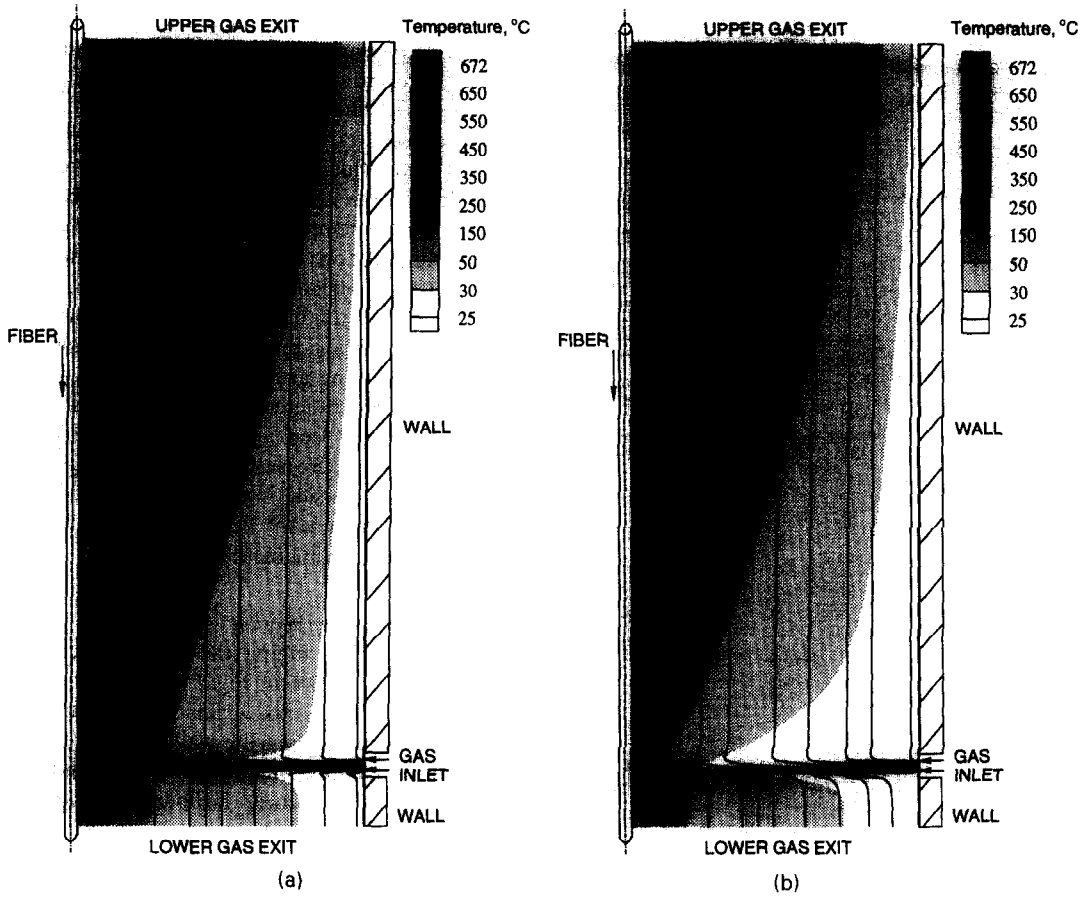

Fig. 5. Streamlines and isotherms for opposing flow ($V_f = 2$ m s^{-1}, $Pe = 350$). (a) $Re = 40$, (b) $Re = 210$.

$40 < Re < 500$, fiber diameter $125 < D_f < 200$ μm and cooling wall diameter 2 mm $< D_w <$ 32 mm. It shows that to a good approximation θ_{out} can be considered independent of T_w and that, in agreement with the experimental observation T_{out} can be taken to vary linearly with T_w.

4.6. *Cooling section performance estimation*

Examination of the expected fiber temperature using a fixed cooling section length leads to the conclusion that as the fiber speed increases it may not be possible to reach acceptable fiber temperatures within the cooling distances involved. Increasing the length

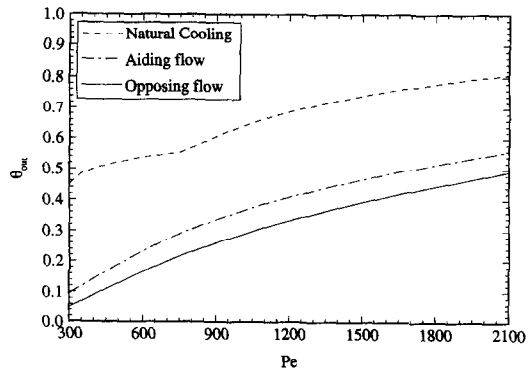

Fig. 6. Effect of Pe for natural cooling as well as opposing and aiding flows.

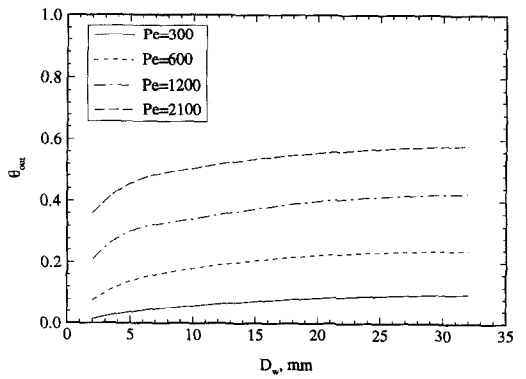

Fig. 7. Opposing flow. Variation of θ_{out} with D_w ($L = 0.604$ m, $D_f = 150$ μm).

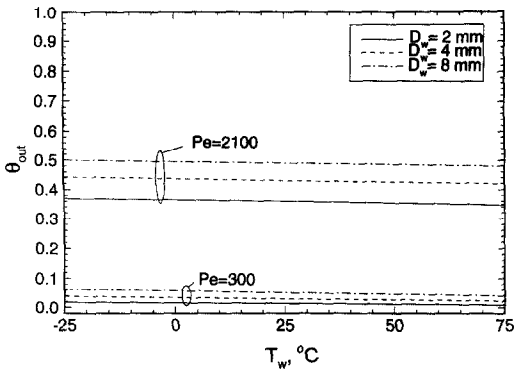

Fig. 8. Opposing flow. Variation of θ_{out} with T_w ($Re = 60$).

of the cooling apparatus offers one possible means of reducing the fiber temperature. The effect of fiber diameter must also be considered, since it affects the mass to be cooled as well as the inlet temperature, T_{fin}.

Figure 9 shows computed values of θ_{out} for opposing flow plotted against Pe for a range of dimensionless cooling section lengths, L', and dimensionless fiber diameters, D_f', which are relevant to the fiber draw process. The results were obtained only for $Re = 60$ and $T_w = 25°C$, since it was previously shown that changes in Re and T_w do not affect θ_{out} considerably. This figure permits fast estimation of the expected fiber exit temperature given the cooling section wall diameter and length, the fiber diameter and speed. The figure also shows that increase of L' causes decrease of θ_{out}, since increasing L' results in increasing the residence time of the fiber inside the cooling section. The effect of fiber diameter can be inferred by comparing values of θ_{out} at the same value of Pe and L' in Fig. 9.

It should be noted that changing the fiber diameter at constant Pe also implies a change in fiber speed, since Pe is proportional to the product of the fiber speed and diameter. The actual effect of a change in fiber diameter, all other conditions remaining the same, is therefore larger than that shown by the change in θ_{out} obtained from Fig. 9 at constant Pe. The actual fiber temperature change following a change in fiber diameter can be obtained by first accounting for the change in Pe, followed by finding the corresponding values of θ_{out} in Fig. 9, and then using the definition of θ_{out} and equation (5) to extract the fiber temperatures from θ_{out}.

Regarding the position of the cooling section the results in refs. [12, 13] have shown that it does not affect θ_{out} and therefore the cooling section can be placed at any convienient position along the fiber path.

4.7. *Effect of variable properties*

Inclusion of variable properties is necessary for accurate model representation of the flow and temperature field. Nevertheless, constant property analysis can also yield reasonable estimation of the fiber exit temperature, θ_{out}, if a proper mean temperature for the gas properties is used. Using variable property model results, the following relation for the mean gas temperature, T_m, was derived:

$$T_m = 0.35 \times \frac{T_{fin} + T_{out}}{2} + 0.65\, T_w. \quad (8)$$

The values of θ_{out}, obtained from the constant property model using relation (8) to estimate the gas properties, were within 10% of those obtained using the variable property model, as Fig. 10 indicates for opposing flows. Equation (8) is also applicable for aiding flows.

5. CONCLUSIONS

An experimental and numerical investigation of forced fiber cooling was performed to assess the influence on the fiber temperature of parameters such as cooling gas flow direction, cooling gas flow rate, fiber speed and diameter, cooling section length and wall diameter and temperature. The gas flow was described using the complete conservation equations with temperature depended properties. The fiber temperature was radially uniform under the small Biot number approximation. Computed fiber temperatures at the cooling apparatus exit were obtained from numerical integration of the conservation equations and were compared with experimental data from a cooling apparatus installed in a fiber draw tower. The agreement between computed and experimental results was very good. This enabled use of computed predictions to assess the effect of a wide variety of operating conditions on the fiber temperature.

For the geometries tested the opposing flows resulted in slightly lower temperatures at the cooling section exit. The effect of gas flow rate, expressed in terms of the Reynolds number, was relatively unimportant. The cooling section distance from the draw tower heater also had a minor influence on the fiber temperature downstream from cooling section. The effect of free convection was also negligible for the geometry and flow conditions considered. The exit fiber temperature increased considerably with fiber speed which was expressed in terms of Pe. The exit fiber temperature also increased with increasing fiber diameter, but decreased as the cooling section diameter decreased. Increasing the length of the cooling apparatus significantly decreased the fiber exit temperature. Comparison between results using variable and constant gas properties yielded an appropriate mean temperature for property estimation for constant property modeling. The results presented allow for the estimation of the fiber exit temperature given the dimensions and the operating conditions of the cooling section.

Acknowledgments—This was was supported by the Fiber Optic Materials Program at Rutgers University and by NSF grant no. DDM-92-13458.

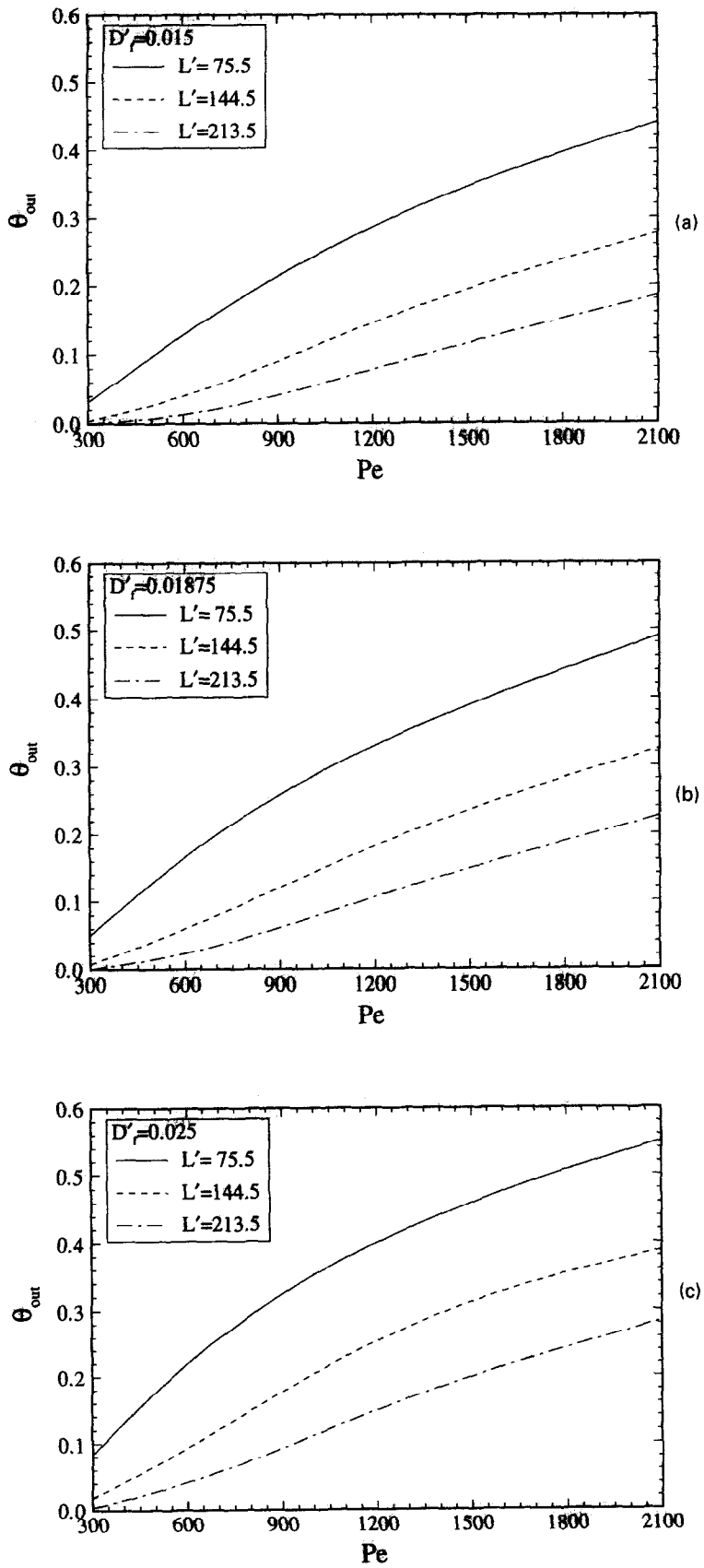

Fig. 9. Opposing flow. Variation of θ_{out} with Pe and L'. (a) $D'_f = 0.015$, (b) $D'_f = 0.01875$, (c) $D'_f = 0.025$.

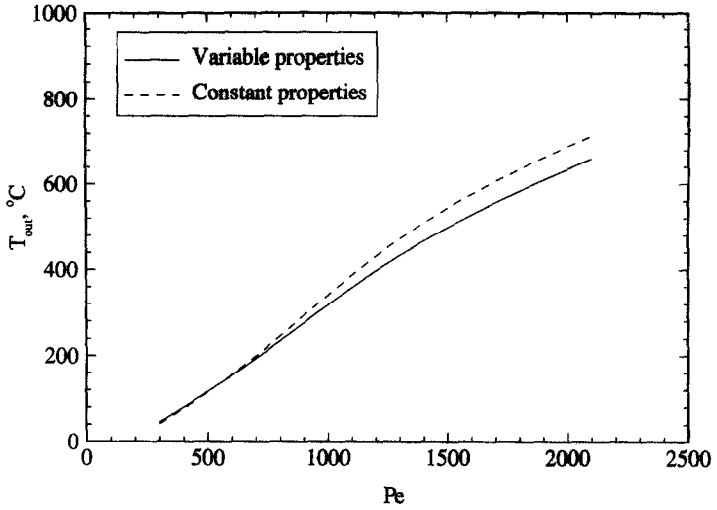

Fig. 10. Opposing flow. Comparison of T_{out} using variable and constant gas properties. ($T_w = 25°C$, $D_w = 8$ mm, $Re = 450$ and helium.)

REFERENCES

1. L. R. Glicksman, The cooling of glass fibres, *Glass Technol.* **9**, 131–138 (1968).
2. D. E. Bourne and D. G. Elliston, 1970, Heat transfer through the axially symmetric boundary layer on a moving circular fibre, *Int. J. Heat Mass Transfer* **13**, 583–593 (1970).
3. D. E. Bourne and H. Dixon, The cooling of fibres in the formation process, *Int. J. Heat Mass Transfer* **24**, 1323–1331 (1971).
4. J. Karniš and V. Pechoč, The thermal boundary layer in a continuous cylinder, *Int. J. Heat Mass Transfer* **21**, 43–47 (1976).
5. R. G. C. Arridge and K. Prior, Cooling times of silica fibres, *Nature* **203**, 386–387 (1964).
6. R Maddison and P. W. McMillan, The cooling rate of glass fibres, *Glass Technol.* **19**, 127–129 (1978).
7. U. C. Paek and C. M. Schroeder, Forced convective cooling of optical fibers in high speed coating, *J. Appl. Phys.* **50**, 6144–6148 (1979).
8. S. Kyriacou, C. E. Polymeropoulos and V. Sernas, Accelerated cooling of optical fiber, *Mater. Res. Soc. Symp. Proc.* **172**, pp. 49–54 (1990).
9. C. M. G. Jochem and J. W. C. Van der Ligt, Cooling and bubble free coating of optical fibers at a high drawing rate, *J. Lightwave Technol.* **LT-4**, 739–744 (1986).
10. V. N. Vasiliev, K. A. Goryachiy, V. D. Noumchik and K. E. Romants, Apparatus for forced cooling of lightguide fiber, *Rev. Higher Educ. Inst.* (Leningrand Institute of Precision Mechanics and Optics, Apparatus Manufacturing) **32**, 90–95 (1989) (in Russian).
11. T. Vaskopulos, C. E. Polymeropoulos and A. Zebib, Heat transfer from optical fiber during the draw process, *J Mater. Process. Manuf. Sci.* **1**, 261–271 (1993).
12. T. Vaskopulos, Forced fiber cooling. Ph.D. Thesis, Rutgers, The State University of New Jersey, New Brunswick, NJ (1994).
13. T. Vaskopulos, C. E. Polymeropoulos and A. Zebib, Heat transfer from a moving surface applied to forced cooling of optical fiber. In *Heat and Mass Transfer in Materials Processing and Manufacturing*, HTD Vol. 261, pp. 21–33. The American Society of Mechanical Engineers, New York (1993).
14. R. S. Choudhury and Y. Jaluria, Forced convective cooling of an optical fiber during thermal processing, *ASME National Heat Transfer Conf. Meet.* Atlanta, GA (1993).
15. B. C. Sakiadis, Boundary layer behaviour on continuous solid surfaces: I. Boundary layer equations for two dimensional and axisymmetric flow, *AIChE J.* **7**, 26–28 (1961).
16. B. C. Sakiadis, Boundary layer behaviour on continuous solid surfaces: II. Boundary layer on a continuous flat surface, *AIChE J.* **7**, 221–225 (1961).
17. B. C. Sakiadis, Boundary layer behaviour on continuous solid surfaces: III. Boundary layer on a continuous cylindrical surface, *AIChE J.* **7**, 467–472 (1961).
18. E. A. Koldenhof, Laminar boundary layers on continuous flat and cylindrical surfaces, *AIChE J.* **9**, 411–418 (1963).
19. J. F. Griffin and J. L. Thorne, On a thermal boundary layer growth on continuous moving belts, *AIChE J.* **13**, 1210–1211 (1967).
20. F. K. Tsou, E. M. Sparrow and R. J. Goldstein, Flow and heat transfer in a boundary layer on a continous moving surface, *Int. J. Heat Mass Transfer* **10**, 219–235 (1967).
21. J. W. Rotte and W. J. Beek, Some models for the calculation of heat transfer coefficients to a moving continuous cylinder, *Chem. Engng Sci.* **24**, 705–716 (1969).
22. K. Chida and Y. Katto, Conjugate heat transfer on continuous moving surfaces, *Int. J. Heat Mass Transfer* **19**, 461–470 (1976).
23. M. V. Karwe and Y. Jaluria, Thermal transport from a heated moving surface, *J. Heat Transfer Trans. ASME* **108**, 728–733 (1986).
24. T. Shigechi and Y. Lee, An analysis of fully developed laminar fluid flow and heat transfer in concentric annuli with moving cores, *Int. J. Heat Mass Transfer* **34**, 2593–2601 (1991).
25. B. H. Kang, Y. Jaluria and M. V. Karwe, Numerical simulation of conjugate transport from a continuous moving plate in materials processing, *Numer. Heat Transfer A* **19**, 151–176 (1991).
26. R. S. Choudhury and Y. Jaluria, Forced convective heat transfer from a continuously moving cylindrical rod undergoing thermal processing. In *Heat Transfer in Materials Processing*, HTD-Vol. 224, pp. 43–50. The

American Society of Mechanical Engineers, New York (1992).
27. R. Siegel and J. R. Howell, *Thermal Radiation Heat Transfer* (2nd Edn). Hemisphere, New York (1981).
28. *Thermophysical Properties of Matter*. IFI Plenum, New York (1970).
29. S. V. Patankar, *Numerical Heat Transfer and Fluid Flow*. Hemisphere, New York (1980).